A phononic band gap model for long bridges. The 'Brabau' bridge case.

G. Carta[a,*], G.F. Giaccu[b], M. Brun[a]

[a] *Dipartimento di Ingegneria Meccanica, Chimica e dei Materiali, Università di Cagliari, 09123 Cagliari (CA), Italy*
[b] *Dipartimento di Architettura, Design e Urbanistica, Università di Sassari, 07041 Alghero (SS), Italy*

Abstract

In this paper, we study the dynamic flexural behavior of a long bridge, modeled as an infinite periodic structure. The analysis is applied to the 'Brabau' bridge across the river Tirso in Italy. The approach reduces to a spectral problem leading to the analytical expression of the dispersion relation, which provides the ranges of frequencies for which waves do and do not propagate. The contributions of the bridge structural elements on the dispersive properties of the structure are investigated in detail. The direct link between frequency intervals determined by the proposed approach and distribution of eigenfrequencies of the full three-dimensional structure is demonstrated. The analysis of the unit cell allows to avoid the tedious computations required when using a finite element code, at least at a preliminary stage of the design. Finally, we demonstrate that a more precise prediction of the eigenfrequency ranges of the bridge can be obtained by studying a single repetitive cell numerically and imposing Floquet-Bloch conditions at its ends. The proposed approach can be implemented as a simple procedure to design structures with repetitive units, with the advantage of simplifying numerical simulations and reducing the computational cost.

Keywords: Multi-span Bridge, Flexural Waves, Dispersion Relation, Structural Dynamics

1. Introduction

Long structures with repetitive units are very common in engineering applications for technological and economical reasons. In fact, in order to make the construction process faster and cheaper, many structures are made of precast elements that are connected *in situ* by appropriate joints. Typical repetitive structures are bridges and viaducts, pipelines and industrial warehouses.

*Corresponding author
Email addresses: giorgio_carta@unica.it (G. Carta), gf.giaccu@uniss.it (G.F. Giaccu), mbrun@unica.it (M. Brun)

'Repetitive structures' with discontinuities or inhomogeneities are characterised by bands of frequencies for which waves travel without attenuation ('propagation ranges') and intervals of frequencies for which waves decay exponentially in space ('non-propagation ranges'). In structures with an infinitely large number of units ('periodic structures'), these frequency bands are denoted as 'pass-bands' and 'stop-bands', respectively. The determination of the non-propagation ranges is of paramount importance in problems of vibration isolation. Indeed, if the repetitive structure is designed such that the frequency components of the external dynamic source (be it traffic, a vibrating machine or an earthquake) lie within the non-propagation ranges of the structure, the amplitudes of the waves generated by the source are significantly attenuated without the need to install dampers.

From the above considerations, we envisage that the availability of a simple modeling tool for the prediction of the non-propagation frequency intervals of a repetitive structure may be of high value for the engineering practice both at the design and verification stages. In particular, long bridges can be efficiently modeled as waveguides representing phononic band gap systems, and the associated dispersion relations enable to deduce the dynamic properties of the vibrating slender structures. A particular feature of the proposed model is the Floquet-Bloch study based on the analysis of a single cell, which drastically simplifies the analytical and numerical modeling of large scale structures and the post-processing analysis.

The first studies on waves in periodic systems date back to the 1950s [1, 2, 3, 4]. Later, one-dimensional elastic structures - such as laminates, assemblies of rods and monodimensional lattices - were investigated by Mead [5], Faulkner and Hong [6], Martinsson and Movchan [7], Brun et al. [8], Carta and Brun [9], Brito-Santana et al. [10]. Lekner [11] examined the propagation of electromagnetic waves in stratified media. Wu et al. [12, 13] used the spectral element method to study the band-gap properties of sandwich panels with corrugated cores and periodic Mindlin plate structures. Hull [14] studied laminated plates by means of a higher-order shear deformation model.

Dynamic properties of beam systems were analysed by Mead [15, 16], Heckl [17], Romeo and Luongo [18], Xu et al. [19]. In this case, the governing equation of motion includes a fourth-order derivative with respect to the spatial coordinate, hence two waves (with or without amplitude attenuation) are expected to travel in each direction. By employing different techniques, Mead [20, 21, 15], Sen Gupta [22, 23], Brun et al. [24] proved that the spectral analysis of Floquet-Bloch waves can be linked directly to the eigenfrequency intervals of a finite real structure. Carta et al. [25, 26] examined the stop-bands and localization phenomena produced by a diffuse damage on a long elastic two-dimensional strip; in addition, they showed that in the low- and medium-frequency regimes the limits of the stop-bands are predicted accurately by means of a lower-dimensional beam model with elastic junctions, the stiffnesses of which can be estimated via asymptotic techniques. A comprehensive analysis of the effects of different geometric distributions of structural elements having discrete and continuum nature is given in [27]. The effects of random perturbations in beam systems

Figure 1: The 'Brabau' bridge across the river Tirso in Oristano, Sardinia, Italy; 39°54'42.5"N 8°32'54.2"E (online version in colour).

were investigated in [28, 29, 30, 31, 32]. Propagation of stable, non-linear waves in periodic buckled beams is discussed in [33, 34], where a parametric resonance model shows that wave propagation depends on pre-compression and dynamic amplitude.

In this paper, we study the dynamics of long bridges with repetitive units. While Floquet-Bloch analysis on periodic structures is known in the literature, its applications in Structural Mechanics are far from being fully exploited, especially as a simple tool for the dynamic design of civil structures. We apply the quasi-periodic analysis to a particular case, namely the road and pedestrian 'Brabau' bridge across the river Tirso in Sardinia, Italy (see Fig. 1). This bridge is made of equally-long spans, consisting of five prestressed concrete beams supported by a dosseret standing on two pillars; the decks of adjacent spans are joined by the only slab in correspondence of the pillars. This construction technology, which ensures the achievement of span lengths up to 30 m, is widespread throughout the world due to its simplicity, speed of execution and relatively low cost. Moreover, the precasting phase guarantees durability and quality of the artifact.

We show that the vibration frequencies of the bridge are confined within specific ranges, which can be estimated through an analytical approach based on the dispersion analysis of the corresponding periodic structure. In particular, we focus our attention on the flexural motion of the bridge. As recommended by European Regulations [35], the vertical component of an earthquake has a relevant importance in case of prestressed concrete bridge decks and, thus, it has to be taken into account for an appropriate design of the structure.

In this work, we provide for the first time an analytical formula, given by Eq. (11), which can be used as a first approximation for the dynamic optimisation of the structure according to the specific demands imposed by the project. Eq. (11) embeds a class of structural parameters which strongly contribute to the dynamic behaviour of the bridge. We show the dynamic effects of these structural parameters and the limitations of the applied formula. Moreover, we provide a complementary simple numerical approach to overcome the limitations of the analytical formulation and to widen the range of applications of the

quasi-periodic analysis to more complicated structural systems.

The paper is organised as follows. In Section 2 we describe the actual bridge and the structural models adopted to investigate its dynamic behavior. In Section 3 we present the analytical method used to predict the eigenfrequency intervals of the bridge, and we discuss how these ranges are affected by the single contributions of the different structural elements. In Section 4 we compare the analytical results with the numerical values obtained from a finite element model, detailing the advantages of the analysis of the single unit cell. We conclude the paper with Section 5, where we provide some concluding remarks.

2. Description of the bridge

The bridge shown in Fig. 1 is located in the west coast of Sardinia, Italy. The structure, which was inaugurated in 2012, connects the city of Oristano with the touristic town of Torregrande.

2.1. Geometric and constitutive properties

The structure of the bridge is shown in Fig. 2. It consists of 41 spans of length $l \simeq 25.4$ m. The elevation of a typical span is 5 m (Fig. 2a). The deck is made of 5 prestressed concrete beams, which in the construction process are assembled by a special crane and subsequently connected to a superior slab, that is designed to resist the horizontal forces transmitted to the main structure by vehicular loads. All the spans are usually pre-designed as simply-supported beams, namely the cross-section and the steel reinforcement are usually calculated conservatively by assuming rigid pillars and pinned connections between the spans, even though in proximity of the pillars the slab generates a structural continuity which reduces the maximum bending moment in the mid-span cross-section. This structural continuity is not taken into account in the static design of the structure, but we will show in Section 4 that it affects significantly the dynamic behavior of the bridge.

The height of the deck is approximately 1.91 m (Fig. 2b). Each beam, including the effective width of the slab (see Fig. 2c), has cross-sectional area $A_0 = 1.14$ m^2 and second moment of inertia $J_0 = 0.52$ m^4. The Young's modulus, Poisson's coefficient and mass density of the deck are given by $E = 34$ GPa, $\nu = 0.2$ and $\rho_0 = 2500$ kg/m^3, respectively. We point out that ρ_0 takes into account also the mass density of the reinforcement.

The deck is sustained by circular pillars of length $l_p \simeq 3.8$ m and diameter $d_p = 1.2$ m (Fig. 2a). The material properties of the pillars are $E_p = 31$ GPa, $\nu_p = 0.2$ and $\rho_p = 2500$ kg/m^3. There are two pillars at each connection, which are joined by a dosseret of mass $m_d = 69300$ kg.

We underline that the constitutive properties of the bridge and their technical characteristics have been ascribed in accordance with the design codes [36] and [37].

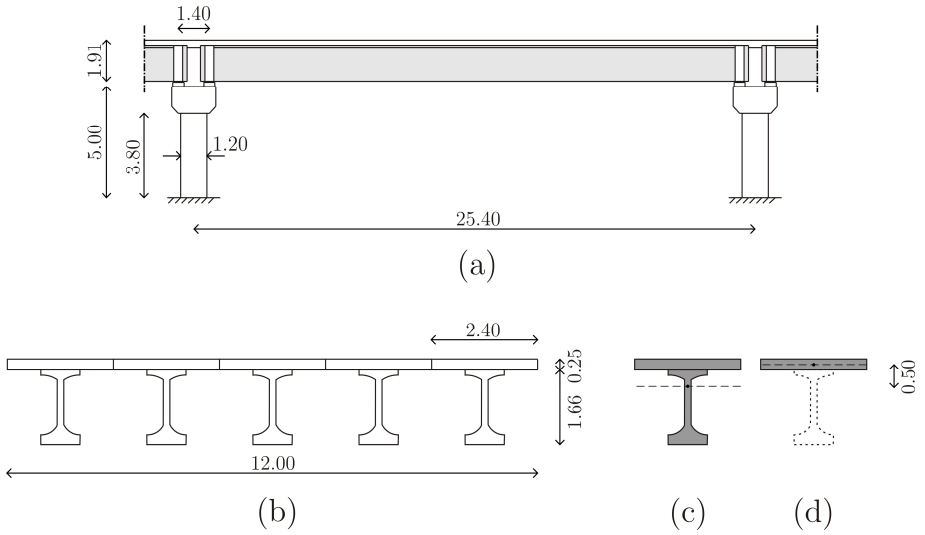

Figure 2: Elevation of a typical bridge span (a); detail of the deck (b); beam cross-section at an internal point of the span (c) and at the junction (d). The dimensions are indicated in m.

2.2. Structural models

The repetitive unit cell of the actual bridge is schematised in Fig. 3a. In proximity of the junction between the main deck and the pillars we consider the change in the cross-section of the deck, as shown in Figs. 2c and 2d. In particular, the centroids of the two cross-sections are at a distance $\bar{h} = 0.50$ m and the length of the bridge region with reduced cross-section is $l_s = 1.40$ m (Figs. 2a and 3a). The two parts of the deck are joined by rigid connectors, indicated by dashed boxes in Fig. 3a. The dosseret is modelled as an horizontal beam rigidly connected to the pillar and joined by hinges to the main deck. The hinges represent the elastomeric bearings, which, for sufficiently low loading values, do not permit relative displacements due to friction. We assume that the dosseret and the foundation are rigid.

We determine the eigenfrequencies of the bridge by implementing the model of Fig. 3a in the commercial finite element software *Strand7*, which is widely used by structural engineers for design purposes. The bridge is modelled as a three-dimensional structure with beam elements, which are commonly employed in the practice. The model is calibrated to take into account the realistic mechanical features of the structure. In particular, infinitely-rigid transverse beams are inserted to ensure the solidity of the deck, according to Courbon's method [38]. In addition, the abutments are idealised as hinges.

Not rarely the structural continuity in proximity of the pillars is restored through a post-tensioning technology. This methodology allows to reach longer spans. For this reason, in this work we have also examined a bridge with a deck made of continuous beams that are rigidly connected to the pillars, as shown in Fig. 3b. In Section 4 we compare the dynamic behaviors of the two bridge

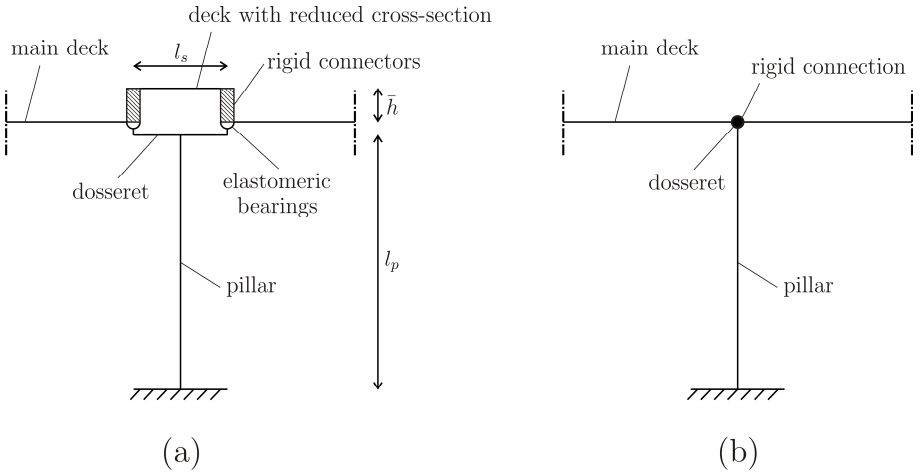

Figure 3: Structural schemes for a repetitive unit of the actual bridge (a) and for a bridge with a continuous beam rigidly connected to the pillars (b).

typologies sketched in Fig. 3. We emphasize that the proposed approach can be applied for any type of connection between the deck and the pillars by varying the bending stiffness of the internal junction.

3. Analytical model of the periodic structure

In this section, we study the repetitive structure of Fig. 1 as a periodic beam placed on elastic supports and with internal elastic connections, as shown in Fig. 4a. The effective properties of the beam representing the upper deck are: Young's modulus E, mass density ρ, cross-sectional area A, second moment of inertia J and span length l. K_B represents the effective bending stiffness of the internal junction modeling the deck region with reduced cross-section, while K_T and K_R denote the effective translational and rotational stiffnesses of the supporting pillars, respectively. In the concentrated mass m we include the inertial effects of the pillars and the dosseret.

Here the foundation is assumed to be rigid. In the case of an elastic foundation of stiffness K_F, the longitudinal stiffness K_T needs to be replaced by $K_T K_F/(K_T + K_F)$.

3.1. Dispersion relation

We consider small amplitude vibrations superimposed on the static displacement due to weight, which is taken as the reference state. Denoting by $v(x)$ the time-harmonic vertical displacement, where x is the spatial coordinate along the beam axis, the equation of motion of the beam between the connections is given by

$$EJv^{IV}(x) - \rho A\omega^2 v(x) = 0, \tag{1}$$

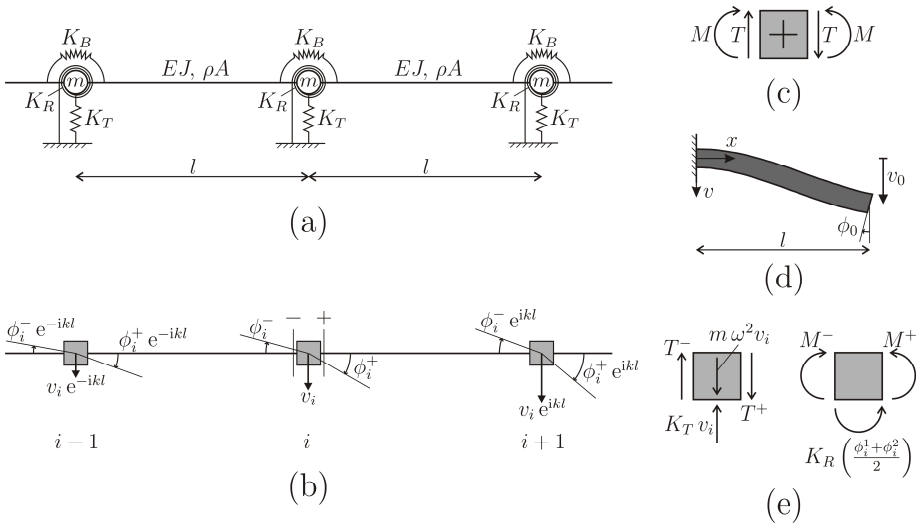

Figure 4: (a) Beam on elastic supports with internal elastic junctions and point masses m at the junction points; (b) quasi-periodic Floquet-Bloch conditions applied to the generic junction node i of the periodic structure; (c) sign conventions for the bending moments and shear forces; (d) simple beam clamped at the left end and with prescribed displacement v_0 and rotation ϕ_0 at the right end; (e) linear and angular momentum balance at node i.

where ω is the radian frequency. The general solution of Eq. (1) can be expressed as

$$v(x) = B_1 \cos(\beta x) + B_2 \sin(\beta x) + B_3 \cosh(\beta x) + B_4 \sinh(\beta x), \tag{2}$$

where $\beta = (\rho A \omega^2 / EJ)^{1/4}$.

Considering the periodicity of the structure, we impose Floquet-Bloch quasi-periodic conditions for the generic nodes $i-1$, i and $i+1$ (see Fig. 4b). In particular, the displacements at nodes $i+1$ and $i-1$ are related to the displacement at node i by the following expressions:

$$v_{i+1} = v_i \mathrm{e}^{\mathrm{i}kl}, \quad v_{i-1} = v_i \mathrm{e}^{-\mathrm{i}kl}. \tag{3}$$

Here, k stands for the wavenumber or Bloch parameter, which defines the phase difference of the displacements calculated at points located at distance l; the wavenumber is associated with the wavelength $\lambda = 2\pi/k$. Similar relations apply to every field, i.e. rotations, bending moments and shear forces. We point out that at the connections the displacements are continuous, while the rotations are generally discontinuous.

In order to determine the bending moments M and shear forces T at the left and right ends of the generic connection i, we compute the constants B_1, B_2, B_3 and B_4 appearing in the solution (2) by referring to a beam with the boundary conditions sketched in Fig. 4d. The sign conventions for bending moments and shear forces are reported in Fig. 4c. The 'dynamic compliance coefficients' at

$x = 0$ and $x = l$ when $v_0 = 1$ and $\phi = 0$ are (see also [39])

$$\begin{aligned} T_0' &= \frac{\beta^3 EJ\left[\sin\left(\beta l\right) + \sinh\left(\beta l\right)\right]}{1 - \cos\left(\beta l\right)\cosh\left(\beta l\right)}, \\ T_l' &= \frac{\beta^3 EJ\left[\cosh\left(\beta l\right)\sin\left(\beta l\right) + \cos\left(\beta l\right)\sinh\left(\beta l\right)\right]}{1 - \cos\left(\beta l\right)\cosh\left(\beta l\right)}, \\ M_0' &= \frac{\beta^2 EJ\left[\cos\left(\beta l\right) - \cosh\left(\beta l\right)\right]}{1 - \cos\left(\beta l\right)\cosh\left(\beta l\right)}, \\ M_l' &= \frac{\beta^2 EJ\sinh\left(\beta l\right)\sin\left(\beta l\right)}{1 - \cos\left(\beta l\right)\cosh\left(\beta l\right)}; \end{aligned} \tag{4}$$

conversely, for $v_0 = 0$ and $\phi = 1$ the compliances are given by

$$\begin{aligned} T_0'' &= \frac{-\beta^2 EJ\left[\cosh\left(\beta l\right) - \cos\left(\beta l\right)\right]}{1 - \cos\left(\beta l\right)\cosh\left(\beta l\right)}, \\ T_l'' &= \frac{-\beta^2 EJ\sinh\left(\beta l\right)\sin\left(\beta l\right)}{1 - \cos\left(\beta l\right)\cosh\left(\beta l\right)}, \\ M_0'' &= \frac{-\beta EJ\left[\sin\left(\beta l\right) - \sinh\left(\beta l\right)\right]}{1 - \cos\left(\beta l\right)\cosh\left(\beta l\right)}, \\ M_l'' &= \frac{-\beta EJ\left[\cosh\left(\beta l\right)\sin\left(\beta l\right) - \cos\left(\beta l\right)\sinh\left(\beta l\right)\right]}{1 - \cos\left(\beta l\right)\cosh\left(\beta l\right)}. \end{aligned} \tag{5}$$

In the quasi-static limit $\omega \to 0$, the dynamic compliance coefficients tend to their static values:

$$\begin{aligned} T_l' \to T_0' &\to \frac{12EJ}{l^3}, \\ M_l' \to -M_0' &\to \frac{6EJ}{l^2}, \\ T_l'' \to T_0'' &\to \frac{-6EJ}{l^2}, \\ M_l'' \to -2M_0'' &\to \frac{-4EJ}{l}. \end{aligned} \tag{6}$$

The bending moments and shear forces at node i (refer to Fig. 4b) are expressed as

$$\begin{aligned} M^- &= M_0'\, v_i\, \mathrm{e}^{-\mathrm{i}kl} + M_l'\, v_i - M_0''\, \phi_i^+\, \mathrm{e}^{-\mathrm{i}kl} + M_l''\, \phi_i^-, \\ M^+ &= M_0'\, v_i\, \mathrm{e}^{\mathrm{i}kl} + M_l'\, v_i + M_0''\, \phi_i^-\, \mathrm{e}^{\mathrm{i}kl} - M_l''\, \phi_i^+, \\ T^- &= -T_0'\, v_i\, \mathrm{e}^{-\mathrm{i}kl} + T_l'\, v_i + T_0''\, \phi_i^+\, \mathrm{e}^{-\mathrm{i}kl} + T_l''\, \phi_i^-, \\ T^+ &= T_0'\, v_i\, \mathrm{e}^{\mathrm{i}kl} - T_l'\, v_i + T_0''\, \phi_i^-\, \mathrm{e}^{\mathrm{i}kl} + T_l''\, \phi_i^+. \end{aligned} \tag{7}$$

Inserting relations (7) into the kinematic compatibility condition

$$\phi_i^+ = \phi_i^- - \frac{M^-}{K_B}, \tag{8}$$

and the balances of linear and angular momentum at node i (see Fig. 4e)

$$\begin{aligned} M^+ &= M^- - K_R \left(\frac{\phi_i^- + \phi_i^+}{2} \right), \\ T^+ &= T^- + \left(K_T - m\,\omega^2 \right) v_i, \end{aligned} \tag{9}$$

where the effect of the rotary inertia of the mass m has been neglected, we obtain the following linear homogeneous system of equations in term of the kinematic variables v_i, ϕ_i^-, ϕ_i^+:

$$\begin{aligned} &\left(\frac{M_0' \mathrm{e}^{-\mathrm{i}kl} + M_l'}{K_B} \right) v_i + \left(\frac{M_l''}{K_B} - 1 \right) \phi_i^- + \left(1 - \frac{M_0'' \mathrm{e}^{-\mathrm{i}kl}}{K_B} \right) \phi_i^+ = 0; \\ &\left[2\,\mathrm{i}\, M_0' \sin\left(kl\right) \right] v_i + \left(M_0'' \mathrm{e}^{\mathrm{i}kl} - M_l'' + \frac{K_R}{2} \right) \phi_i^- \\ &+ \left(M_0'' \mathrm{e}^{-\mathrm{i}kl} - M_l'' + \frac{K_R}{2} \right) \phi_i^+ = 0; \\ &\left[2\,T_0' \cos\left(kl\right) - 2\,T_l' - K_T + m\,\omega^2 \right] v_i + \left(T_0'' \mathrm{e}^{\mathrm{i}kl} - T_l'' \right) \phi_i^- \\ &+ \left(T_l'' - T_0'' \mathrm{e}^{-\mathrm{i}kl} \right) \phi_i^+ = 0. \end{aligned} \tag{10}$$

The condition for a non-trivial solution of system (10) is the dispersion relation for the periodic beam in Fig. 4a, which is given by

$$\begin{aligned} &\frac{2\,T_l''}{K_B} \left[M_l' M_l'' - M_0' M_0'' + \cos\left(kl\right) \left(M_0' M_l'' - M_l' M_0'' \right) - \frac{K_R}{2} \left(M_l' + M_0' \mathrm{e}^{-\mathrm{i}kl} \right) \right] \\ &+ 2\,T_0'' \left\{ 2\,M_0' \sin^2\left(kl\right) - \frac{1}{K_B} \left[M_0' M_l'' - M_l' M_0'' + \cos\left(kl\right) \left(M_l' M_l'' - M_0' M_0'' \right) \right. \right. \\ &\left. \left. - \frac{K_R}{2} \cos\left(kl\right) \left(M_l' + M_0' \mathrm{e}^{-\mathrm{i}kl} \right) \right] \right\} + \left[2\,\cos\left(kl\right) T_0' - 2\,T_l' + m\,\omega^2 - K_T \right] \\ &\times \left[2\,\cos\left(kl\right) M_0'' - 2\,M_l'' + \frac{M_l''^2 - M_0''^2}{K_B} - K_R \left(\frac{M_l'' + M_0'' \mathrm{e}^{-\mathrm{i}kl}}{2\,K_B} - 1 \right) \right] = 0. \end{aligned} \tag{11}$$

It is evident that the transcendental dispersion relation (11), relating the frequency ω (also embedded in the parameter β) to the wavenumber k, depends on the stiffnesses of the supporting pillars K_R and K_T, the lumped mass m and the bending stiffness of the connection K_B. In the next subsection, we describe the separate effects of these four quantities on the dispersive properties of the periodic beam.

3.2. Effects of structural parameters on dispersion properties

We introduce the non-dimensional stiffness ratios $\chi_R = K_R l/EJ$, $\chi_T = K_T l^3/EJ$, $\chi_B = K_B l/EJ$ and the non-dimensional mass ratio $\chi_m = m/\rho A l$. Consequently, we express the dispersion relation (11) in terms of the non-dimensional frequency parameter $\bar{\beta} = \beta l$ and non-dimensional Bloch-parameter

$\bar{k} = kl$. In Fig. 5 we show in black colour the dispersion curves of the beam in the $\bar{\beta}$-$\bar{k}$ plane, highlighting the contributions of χ_R, χ_T, χ_m and χ_B taken separately. The grey lines represent instead the dispersion curves for a homogenoeus beam without supports ($\chi_R = \chi_T = \chi_m = 0$) or cross-section discontinuity ($\chi_B \to \infty$).

For the continuous beam without supports the dispersion curves $\bar{\beta} = \pm\bar{k} + 2n\pi$ (n positive integer) do not exhibit stop-bands [40], which implies that waves of any frequency can travel in the structure without attenuation. Conversely, the presence of inhomogeneities in the form of elastic supports or internal junctions open stop-bands at specific frequencies. More specifically, the introduction of the rotational stiffness of the pillars (Fig. 5a) lifts up the lower limits of the optical branches without influencing the frequency interval of the low-frequency acoustic branch (the solution $\omega = 0$, $k = 0$ can be easily retrieved from the dispersion relation (11)). In addition, the group velocity, describing energy propagation and associated to the slope of the dispersion curves, is null at each band limit.

We also note a stiffening effect in the quasi-static limit ($\bar{\beta}$, $\bar{k} \to 0$), where the dispersion relation takes the form

$$\omega^2 = \frac{EJ}{\rho A}\frac{1}{1+\chi_m}\frac{12\chi_R}{12+\chi_R}k^2. \tag{12}$$

On the other hand, the dispersion relation for a homogeneous beam is given by $\omega^2 = (EJ/\rho A)k^4$. Eq. (12) has the same structure, with different structural parameters, as the dispersion curve associated with longitudinal waves, which are governed by a second-order harmonic equation.

The longitudinal stiffness of the pillars χ_T (Fig. 5b) leads to similar effects concerning optical branches, but mainly gives rise to a cut-off frequency below which waves cannot propagate, opening a band gap at zero frequency. We also note that there is an optimal stiffness for which the frequency interval associated to the acoustic branch becomes negligibly small. An increase of the stiffness above the optimal value is not beneficial in terms of wave filtering.

Both the point mass m (Fig. 5c) and the elastic junction described by χ_B (Fig. 5d) open band gaps. The main effect is the decrease in the upper limits of both acoustical and optical branches.

The above discussion should give clear indications to the engineer on how to modify the limits of the stop-bands, in accordance with the design demands. In particular, it appears that the principal contribution is given by the longitudinal stiffness of the supporting pillars, which opens a band gap at zero frequency and has a quantitatively greater influence on the widths of the pass-bands. The effects of rotational stiffness and pillars inertial contribution can be used to modulate the pass-band opening. In terms of possible technological applications, we stress that longitudinal and rotational equivalent stiffnesses of the supporting pillars, i.e. χ_T and χ_R, can be strongly influenced by the introduction of *ad hoc* bearing elements at the junctions between the pillars and the upper deck of the bridge.

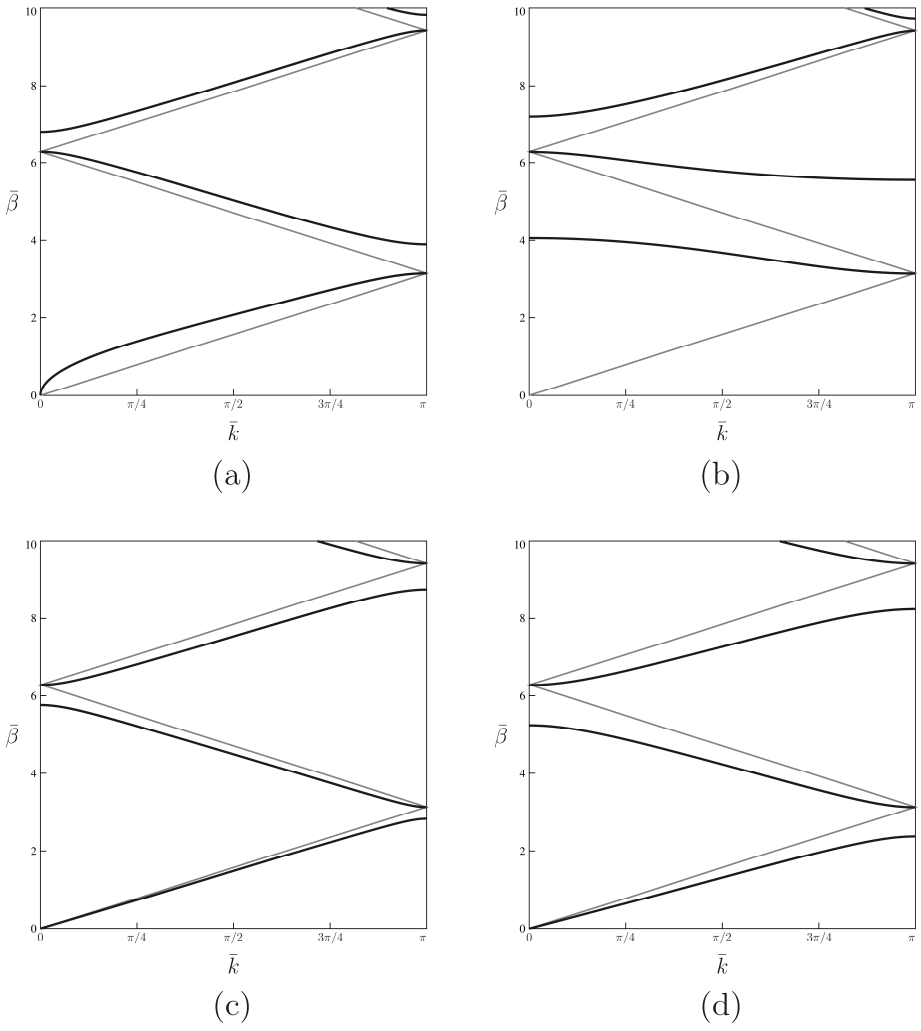

Figure 5: Dispersion curves for the periodic structure, obtained from Eq. (11). In black colour: (a) $\chi_R = 10$, $\chi_T = \chi_m = 0$, $\chi_B \to \infty$; (b) $\chi_T = 500$, $\chi_R = \chi_m = 0$, $\chi_B \to \infty$; (c) $\chi_m = 0.25$, $\chi_R = \chi_T = 0$, $\chi_B \to \infty$; (d) $\chi_R = \chi_T = \chi_m = 0$, $\chi_B = 1$. In grey colour: $\chi_R = \chi_T = \chi_m = 0$, $\chi_B \to \infty$.

4. Dynamic study of the bridge

The dispersion analysis developed in Section 3 is relevant to periodic structures, namely structures with an infinite number of repetitive units. The bridge described in Section 2 is instead a structure with a finite number of spans. In this section we show that the finite and periodic models are related to each other, since the eigenfrequencies of the finite bridge fall inside the pass-bands of the periodic structure.

4.1. Bridge with rigid deck-pillars connections

We start by examining a continuous model of the bridge, in which the deck and the pillars are rigidly connected, as in Fig. 3b. The rotational and translational rigidity of the two supporting pillars are evaluated as

$$K_R = \frac{E_p J_p}{l_p} \tag{13}$$

and

$$K_T = \frac{E_p A_p}{l_p}, \tag{14}$$

respectively, while the concentrated mass m is given by

$$m = \frac{\rho_p A_p l_p}{2} + m_d. \tag{15}$$

In Eqs. (13)-(15) E_p, ρ_p, l_p, A_p and J_p are respectively the Young's modulus, the mass density, the length, the total area and the total second moment of inertia of the two pillars, while m_d is the mass of the dosseret. Expressions (13) and (14) correspond to the flexural and longitudinal rigidities of a clamped beam, while the equivalent mass in (15) has been determined evaluating the kinetic energy of the supporting pillars and the dosseret. In this model, the bending stiffness of the connection $K_B \to \infty$.

We determine the eigenfrequencies of the bridge associated with flexural modes by using the finite element model described in Section 2.2. For the purpose of illustration, we consider three bridge structures with different numbers of spans: 5, 10 and 15. We report the corresponding eigenfrequencies for $\omega \leq 400$ rad/s on the right of Fig. 6, where they are indicated by dots.

The first three dispersion curves of the periodic analytical model, derived from Eq. (11), are plotted in solid line in Fig. 6, where the horizontal dashed lines indicate the limits of the analytical pass-bands. From Fig. 6 it is apparent that the eigenfrequencies of the finite structure lie within well-defined frequency intervals, that correspond to the pass-bands of the periodic model. The agreement is excellent for the first two bands, while the small differences in the third band are due to the approximation of the analytical mono-dimensional beam model, which loses accuracy at higher frequencies with respect to the behavior of a three-dimensional structure. Finally, we note that the number of eigenfrequencies in each pass-band coincides with the number of spans.

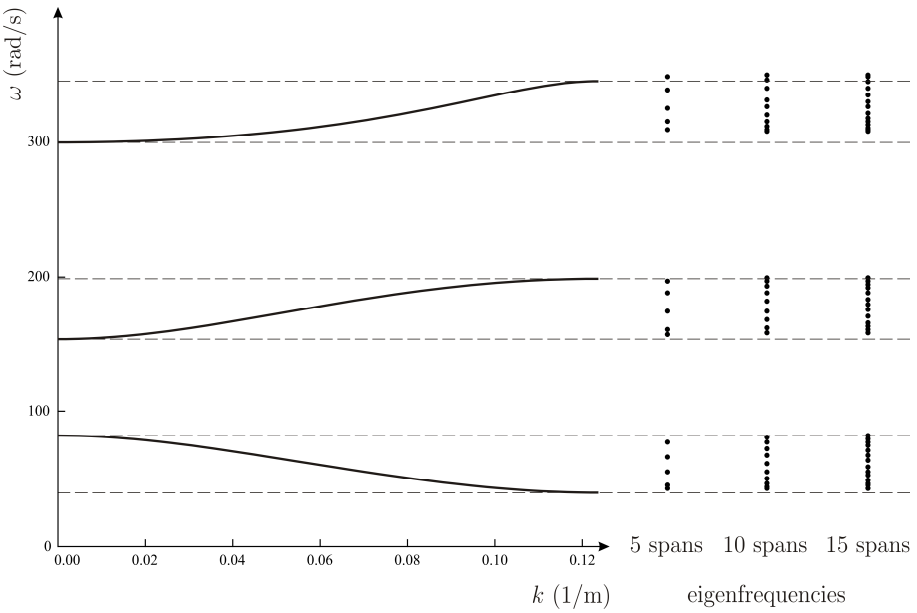

Figure 6: Dispersion curves (solid lines) for a periodic bridge with rigid deck-pillars connections (see Fig. 3b) and eigenfrequencies (dots) for the analogous finite bridge with 5, 10 and 15 spans, determined with *Strand7*.

The percent differences between the limits of the pass-bands determined analytically and the bounding frequencies computed numerically are reported in Table 1. The percent differences Δ are calculated with the following formula:

$$\Delta = \frac{\omega_{\mathrm{AN}} - \omega_{\mathrm{FE}}}{\omega_{\mathrm{FE}}} \times 100, \tag{16}$$

where ω_{AN} is the limit of the pass-band predicted analytically, while ω_{FE} is the bounding frequency determined with the finite element model. The numerical values confirm the good agreement between Floquet-Bloch and eigenfrequency analyses; the larger differences relative to the first pass-band can be attributed to the smaller value of the frequency in the denominator of Eq. (16).

4.2. Bridge with internal elastic junctions

Here we consider the more accurate model of the real bridge, which consists of simply-supported decks connected only by the slab in correspondence of the pillars (Fig. 3a). The connection due to the slab is represented by a rotational spring of stiffness K_B (Fig. 4a).

In order to evaluate K_B we study the frame in Fig. 7, which resembles the structural scheme in Fig. 3a. We recall that $\bar{h}$ is the distance between the centroids of the deck and of the slab, while E_s, l_s, b_s, h_s, $A_s = b_s h_s$ and $J_s = b_s h_s^3/12$ are the elastic modulus, the length, the width, the height, the

Table 1: Percent differences Δ between the limits of the pass-bands predicted by means of the analytical approach and the bounding frequencies of the finite structures with different spans computed numerically, for the case of rigid connections.

pass-band	limit	5 spans	10 spans	15 spans
1	inf $(k = \pi/l)$	-6.95%	-7.81%	-8.02%
	sup $(k = 0)$	6.14%	1.42%	0.67%
2	inf $(k = 0)$	-2.23%	-2.85%	-2.85%
	sup $(k = \pi/l)$	0.92%	-0.59%	-0.59%
3	inf $(k = 0)$	-3.23%	-2.60%	-2.60%
	sup $(k = \pi/l)$	-1.05%	-1.33%	-1.33%

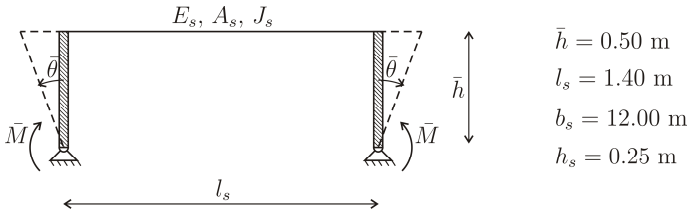

Figure 7: Structural model of the connection between the decks due to the slab.

area and the second moment of inertia of the slab. The values of $\bar{h}$, l_s, b_s and h_s are reported on the right of Fig. 7. The columns of the frame are assumed to be infinitely rigid. Simple calculations yield

$$K_B = \frac{\bar{M}}{\bar{\theta}} = \frac{2\,E_s\left(J_s + A_s\bar{h}^2\right)}{l_s}. \tag{17}$$

The dispersion curves of the periodic analytical model with internal elastic connections are obtained from Eq. (11) by using the formulae (13)-(15) and (17). They are indicated in solid line in Fig. 8, together with their limits in dashed line. On the right of Fig. 8 we include the eigenfrequencies of the finite element model with 5, 10, 15 and 41 spans (the latter represents the real bridge).

By comparing Figs. 8 and 6, we observe that the ranges of eigenfrequencies shrink if rigid connections are substituted by elastic junctions, consistently with the results shown in Fig. 5d. We point out that, while the junction is designed to sustain static loads, it can also be considered as a structural system that can be implemented to limit propagation of dynamic excitation within the bridge. The periodic analysis on a single cell provides an efficient tool to achieve such a design goal.

Fig. 8 shows that the first range of eigenfrequencies, which is the most important one for practical applications, is obtained with high accuracy. At higher frequency the results are less accurate. The loss of precision is expected considering the higher complexity of the model with elastic junctions and the difficulty in assessing the bending stiffness of the connections. Nevertheless,

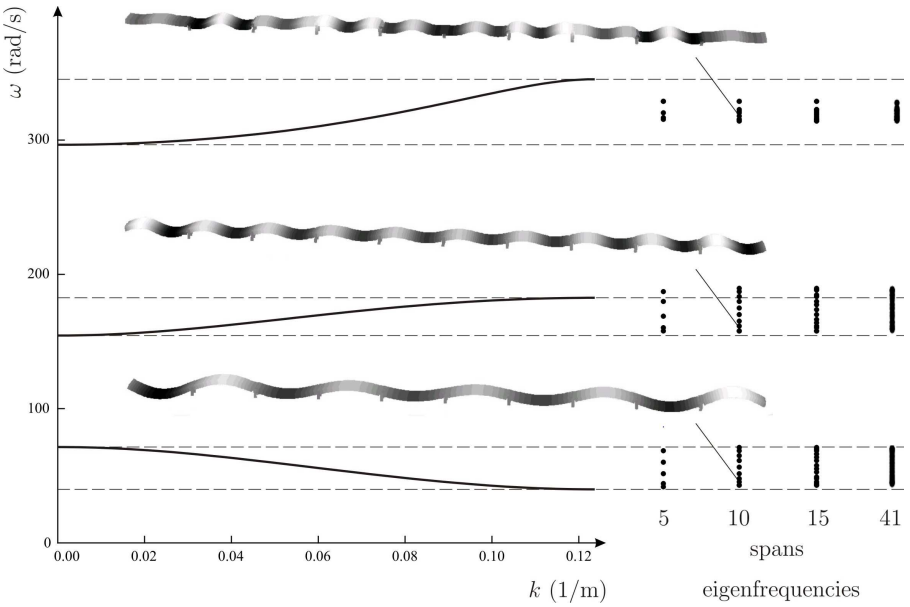

Figure 8: Analytical dispersion curves (solid lines) for a periodic bridge with internal elastic junctions (refer to Fig. 3a) and eigenfrequencies (dots) for the actual bridge with 5, 10, 15 and 41 spans computed with *Strand7*. Some examples of the structural modes obtained with *Strand7* and relative to the bridge with 10 spans are also illustrated.

Table 2: Percent differences Δ obtained from Eq. (16) between the limits of the pass-bands estimated analytically and the bounding frequencies of the finite structures determined numerically, for the case of elastic connections.

pass-band	limit	5 spans	10 spans	15 spans	41 spans
1	inf $(k = \pi/l)$	-4.95%	-5.85%	-6.07%	-6.07%
	sup $(k = 0)$	4.32%	0.65%	-0.06%	-0.06%
2	inf $(k = 0)$	-2.23%	-2.23%	-2.23%	-2.23%
	sup $(k = \pi/l)$	-2.36%	-3.91%	-3.91%	-3.91%
3	inf $(k = 0)$	-5.86%	-5.56%	-5.56%	-5.56%
	sup $(k = \pi/l)$	4.97%	4.97%	4.97%	4.97%

we notice that the eigenfrequencies tend to accumulate within well-defined frequency intervals, which correspond to the pass-bands of the periodic structure and can be determined by a more accurate analytical or numerical model of the unit cell. Table 2 shows the percent differences Δ between the limits of the pass-bands calculated analytically and the bounding frequencies found numerically. We observe that there are no differences between the structures with 15 and 41 spans.

In order to obtain more accurate dispersion curves, we build a finite element model of the periodic unit of the bridge, imposing quasi-periodicity Floquet-Bloch conditions at its left and right boundaries. For this purpose, we use the software *Comsol Multiphysics* (version 4.3b), which allows the implementation of quasi-periodic boundary conditions. The determination of the dispersion curves through this numerical model requires the implementation of a single unit cell instead of the whole structure. The numerical dispersion curves are reported in grey colour in Fig. 9, together with the eigenfrequencies of the finite bridges indicated by black dots, which are identical to those in Fig. 8. The comparative analysis between the numerical periodic and finite models reveals the excellent agreement between eigenfrequency distribution and frequency intervals obtained numerically by studying a single unit cell. The percent differences are reported in Table 3. They are calculated with this formula:

$$\Delta^* = \frac{\omega_{\text{per}} - \omega_{\text{fin}}}{\omega_{\text{fin}}} \times 100, \tag{18}$$

where ω_{per} is the limit of the pass-band for the periodic system and ω_{fin} is the bounding frequency of the finite structure.

The limits of the pass-bands for the periodic system can be predicted by imposing specific boundary conditions at the ends of the elementary cell, considered as a finite structure. In particular, the limits of the first and third pass-bands coincide with the first four eigenfrequencies of a single isolated elementary cell with sliders at the ends, corresponding to zero rotations and equal and opposite displacements at $k = 0$ and $k = \pi/l$, respectively. The limits of the second pass-band are equal to the first two natural frequencies of the elementary cell with hinges at its boundaries, corresponding to zero displacements

Table 3: Percent differences Δ^* between the limits of the pass-bands of the periodic system and the bounding frequencies of the finite structures with different spans, both determined numerically.

pass-band	limit	5 spans	10 spans	15 spans	41 spans
1	inf $(k = \pi/l)$	2.62%	1.65%	1.41%	1.41%
	sup $(k = 0)$	4.82%	1.13%	0.42%	0.42%
2	inf $(k = 0)$	0.44%	0.44%	0.44%	0.44%
	sup $(k = \pi/l)$	1.50%	-0.11%	-0.11%	-0.11%
3	inf $(k = 0)$	-0.19%	0.13%	0.13%	0.13%
	sup $(k = \pi/l)$	0.76%	0.76%	0.76%	0.76%

and equal and opposite rotations at $k = 0$ and $k = \pi/l$, respectively. The eigenmodes computed at $k = 0$ and $k = \pi/l$, which are illustrated in Fig. 9, provide a clear indication of the boundary conditions to apply at the ends of the elementary cell to predict the limits of the pass-bands.

4.3. Bridge with simple supports

We also study the special case of a continuous bridge over periodic supports, for which an analytical expression of the pass-bands and stop-bands is given in the literature [22].

The solid lines in the left diagram of Fig. 10 represent the dispersion curves obtained from the analytical approach presented in this paper, which are calculated from Eq. (11) after substituting $m = 0$, $K_R = 0$, $K_T \to \infty$ and $K_B \to \infty$. In the same diagram, the dots are the numerical values determined with the three-dimensional finite element model of a periodic cell of the bridge, developed in *Comsol Multiphysics*. It is apparent that there is a perfect correspondence between analytical and numerical results.

The pass- and stop-bands of a periodically-supported beam can be calculated by using the following expression [22]:

$$\cosh(\mu) = -\frac{\cot(\beta l) - \coth(\beta l)}{\operatorname{cosech}(\beta l) - \operatorname{cosec}(\beta l)}, \tag{19}$$

where l is the distance between the supports, $\beta = (\rho A \omega^2 / EJ)^{1/4}$ and μ is the propagation constant, which is related to the decay of wave amplitudes. In particular, the real part of μ is used to determine the pass- and stop-bands for the structure: if $\mu = 0$ waves propagate without attenuation (pass-bands), while if $\mu > 0$ waves decay exponentially (stop-bands). In the right diagram of Fig. 10 we plot the propagation constant μ in relation with the radian frequency ω. An expression similar to (19) is obtained in [24] by means of the Green's function method.

The horizontal dashed lines in Fig. 10 indicate the limits of the pass-bands. The comparison between the two diagrams shows that the results of our analytical method and our numerical model agree perfectly with the analytical

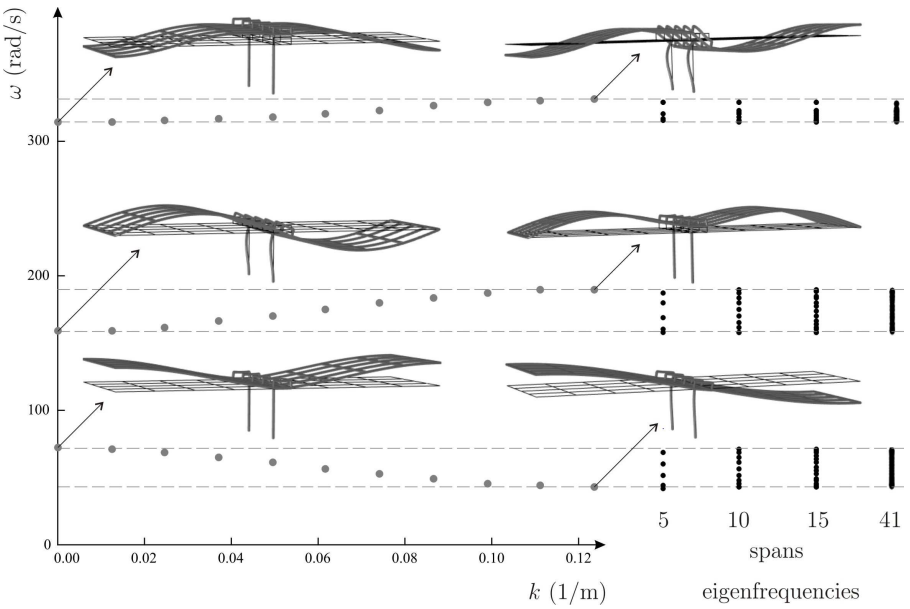

Figure 9: Grey colour: numerical dispersion curves derived from *Comsol Multiphysics* by applying Floquet-Bloch conditions to a periodic unit of the real bridge with elastic junctions; some instances of the eigenmodes of the structure are also presented. Black colour: eigenfrequencies of the actual bridge with a finite number of spans, determined with *Strand7*.

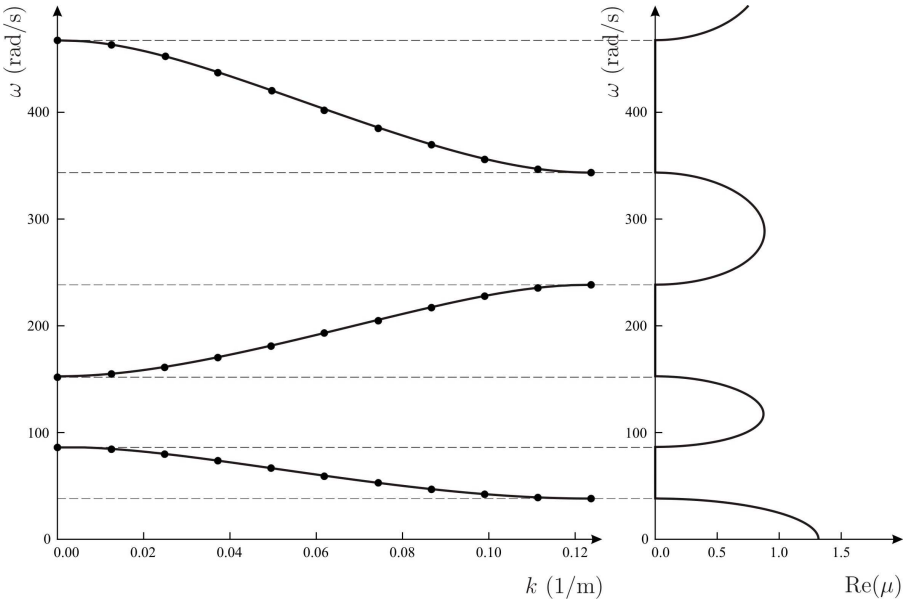

Figure 10: Dispersion curves for a three-dimensional bridge with periodic supports, obtained from Eq. (11) (solid lines) and from the numerical model built in *Comsol Multiphysics* (dots); variation of the real part of the propagation constant μ with the angular frequency ω, given by Eq. (19). The horizontal dashed lines represent the limits of the pass-bands for the two diagrams, which coincide.

approach presented in [22]. This comparative study confirms the validity of our approach.

Experimental results on simply-supported [41] and binary [42] repetitive beams show the agreement between theoretical predictions and experimental outcomes.

5. Conclusions

The dispersion analysis is a powerful tool for the design of repetitive structures, as it quickly provides the frequency ranges for which waves can or cannot propagate without the need to analyse the full structure and to use a finite element model. In this paper, we have employed the dispersion analysis to derive the formula (11), which allows to estimate the positions and the widths of the pass-bands of a complicated periodic structure, such as a long bridge. The main benefit of Eq. (11) is that it quickly provides the intervals of natural frequencies of a repetitive structure, which are very difficult to obtain especially when the structure consists of more than 30 units. Moreover, in the analysis presented in Section 3.2 we have illustrated the influence of each single structural element on the dynamic properties of the whole structure. In particular, we have found that the major contribution is from the longitudinal stiffness of the pillars, which strongly affects the limits of the pass-bands. The contributions of the main structural elements are included in Eq. (11), which can be easily used by the designer at the pre-design stage of the project to tune the dynamic response of the system by varying the proper parameters. The limits of the pass-bands can be also assessed by studying a single isolated repetitive unit and imposing the appropriate boundary conditions at the ends. After determining the geometric and material properties that need to be assigned to the structure to satisfy specific demands, the designer could improve the results by building a finite element model of the system and calculating the eigenfrequencies numerically.

The dispersion relation (11) contains quantities (such as the stiffnesses of the pillars and of the elastic connections) that need to be evaluated *a priori*, either analytically as in Eqs. (13)-(17) or carrying out simple static finite element computations. The latter generally yield more precise results, but require additional numerical work.

In the majority of cases, the eigenfrequency intervals of the structure are predicted with sufficient accuracy by the analytical formula (11). To estimate the eigenfrequency ranges of the repetitive structure more precisely, it is also possible to analyse the periodic structure numerically, performing a finite element eigenfrequency analysis on a single unit cell of the structure subjected to Floquet-Bloch quasi-periodicity conditions applied at its boundaries. Following this approach only a single cell needs to be implemented, drastically reducing the number of degrees of freedom with respect to the implementation of the whole structure and simplifying the post-processing visualisation and data interpretation. The reported eigenfrequency analysis of the whole bridge with 41 spans has pointed out numerical issues, which are avoided by the quasi-periodic

analysis of a single cell. In particular, in the finite element modal analysis of the real bridge with 41 units we have experienced several convergence problems, hence we had to tune the number of iterations and the convergence tolerance for the Sub-Space Iteration Method giving the extremely close eigenfrequencies and the corresponding eigenmodes; in addition, in view of the large number of modes, we had to subdivide the modal analysis into several different steps starting from different minimum frequencies.

The analysis of the 'Brabau' bridge has shown the applicability of the proposed methodology and particular aspects that require special attention when a real structure is considered. Of course, the periodic analysis contains some intrinsic limitations. For example, it cannot be used to calculate the exact values of all the eigenfrequencies of the bridge. However, as the number of spans is increased, the eigenfrequencies cover completely the pass-bands of the corresponding periodic structure. Furthermore, a more sophisticated analysis is required when uncertainties are included into the analytical formulation. These uncertainties concern the geometric and material properties of the bridge but not the loads, which are not relevant in the dynamic characterisation of the structure. A disordered or perturbed system can be studied by introducing random parameters when defining the properties of the structure. The main effect of random perturbations is generally to decrease the propagation ranges and to create localised modes within the system [28, 29, 30, 31, 32]. A detailed analysis of the 'Brabau' bridge under perturbed conditions will be carried out in a future work. We also plan to carry out an experimental validation of the bridge in a future investigation, first by building a scaled model in the lab and then by extrapolating dynamic data from the real structure.

Finally, we point out that in this paper we have considered only the flexural modes of the structure. An analogous formulation can be easily developed for axial, torsional or other vibration modes by substituting Eq. (1) with the proper equations of motion.

Acknowledgements

The authors are grateful to Eng. Marco Manai at the Provincia di Oristano for kindly supplying them with the design data of the examined bridge, and to Prof. Andrea Paglietti for the precious suggestions on the paper. The authors acknowledge the financial support of Regione Autonoma della Sardegna (LR7 2010, grant 'M4' CRP-27585). G.F.G. would like to acknowledge also the financial support of Regione Autonoma della Sardegna (L.R. n. 3/2008 "Rientro Cervelli" and L.R. n. 7/2007 "Promozione della Ricerca Scientifica e dell'Innovazione Tecnologica in Sardegna").

References

[1] Brillouin L. Wave propagation in periodic structures: Electric filters and crystal lattices. 1st ed. New York: McGraw-Hill; 1946.

[2] Brekhovskikh LM. Reflection of Plane Waves from Layered Inhomogeneous Media. J Tech Phys (USSR) 1949;19:1126-1135 (in Russian).

[3] Kittel C. Introduction to solid state physics. 1st ed. New York: John Wiley & Sons; 1953.

[4] Ewing MW., Jardetzky WS. Elastic Waves in Layered Media, McGraw Hill, New York; 1957.

[5] Mead DJ. Wave propagation and natural modes in periodic systems: I. Mono-coupled systems. J Sound Vib 1975; 40:1-18.

[6] Faulkner MG, Hong DP. Free vibrations of a mono-coupled periodic system. J Sound Vib 1985;99:29-42.

[7] Martinsson PG, Movchan AB. Vibrations of lattice structures and phononic band gaps. Q J Mech Appl Math 2002;56:45-64.

[8] Brun M, Guenneau S, Movchan AB, Bigoni D. Dynamics of structural interfaces: Filtering and focussing effects for elastic waves. J Mech Phys Solids 2010;58:1212-1224.

[9] Carta G, Brun M. A dispersive homogenization model based on lattice approximation for the prediction of wave motion in laminates. J Appl Mech 2012;79:021019.

[10] Brito-Santana H, Wang YS, Rodriguez-Ramos R, Bravo-Castillero J, Guinovart-Diaz R, Tita V. A dispersive nonlocal model for shear wave propagation in laminated composites with periodic structures. Eur J Mech A/Solids 2015;49:35-48.

[11] Lekner J. Light in periodically stratified media. J Opt Soc Am A 1994;11:2892-2899.

[12] Wu ZJ, Li FM, Wang YZ. Vibration band gap behaviors of sandwich panels with corrugated cores. Comput Struct 2013;129:30-39.

[13] Wu ZJ, Li FM, Wang YZ. Vibration band gap properties of periodic Mindlin plate structure using the spectral element method. Meccanica 2014;49:725-737.

[14] Hull AJ. A higher-order shear deformation model of a periodically sectioned plate. J Vib Acoust 2016;138:051010.

[15] Mead DJ. Wave propagation and natural modes in periodic systems: II. Multi-coupled systems, with and without damping. J Sound Vib 1975;40:19-39.

[16] Mead DJ. Wave propagation in continuous periodic structures: research contributions from Southampton, 1964-1995. J Sound Vib 1996;190:495-524.

[17] Heckl MA. Coupled waves on a periodically supported Timoshenko beam. J Sound Vib 2002;252:849-882.

[18] Romeo F, Luongo A. Invariants representation of propagation properties for bi-coupled periodic structures. J Sound Vib 2002;257:869-886.

[19] Xu Y, Zhou X, Wang W, Wang L, Peng F, Li B. On natural frequencies of non-uniform beams modulated by finite periodic cells. Phys Lett A 2016;380:3278-3283.

[20] Mead DJ. Free wave propagation in periodically supported, infinite beams. J Sound Vib 1970;11:181-197.

[21] Mead DJ. A general theory of harmonic wave propagation in linear periodic systems with multiple coupling. J Sound Vib 1973;27:235-260.

[22] Sen Gupta G. Natural flexural waves and the normal modes of periodically-supported beams and plates. J Sound Vib 1970;13:89-101.

[23] Sen Gupta G. Natural frequencies of periodic skin-stringer structures using a wave approach. J Sound Vib 1971;16:567-580.

[24] Brun M, Giaccu GF, Movchan AB, Movchan NV. Asymptotics of eigenfrequencies in the dynamic response of elongated multi-structures. Proc Royal Soc A 2011;468:378-394.

[25] Carta G, Brun M, Movchan AB. Dynamic response and localisation in strongly damaged waveguides. Proc Royal Soc A 2014;470:20140136.

[26] Carta G, Brun M, Movchan AB. Elastic wave propagation and stop-band generation in strongly damaged solids. Fract Struct Int 2014;29:28-36.

[27] Carta G, Brun M. Bloch-Floquet waves in flexural systems with continuous and discrete elements. Mech Mat 2015;87:11-26.

[28] Castanier MP, Pierre C. Lyapunov exponents and localization phenomena in multi-coupled nearly periodic systems. J Sound Vib 1995;183:493-515.

[29] Ariaratnam ST, Xie WC. Wave localization in randomly disordered nearly periodic long continuous beams. J Sound Vib 1995;181:7-22.

[30] Bouzit D, Pierre C. Wave localization and conversion phenomena in multi-coupled multi-span beams. Chaos Sol Fract 2000;11:1575-1596.

[31] Li FM, Wang YS, Hu C, Huang WH. Localization of elastic waves in randomly disordered multi-coupled multi-span beams. Waves Random Complex Media 2004;14:217-227.

[32] Carta G, Brun M, Movchan AB, Boiko, T. Transmission and localisation in ordered and randomly-perturbed structured flexural systems. Int J Eng Sci 2016;98:126-152.

[33] Maurin F, Spadoni A. Wave propagation in periodic buckled beams. Part I: Analytical models and numerical simulations. Wave Motion 2016;66:190-209.

[34] Maurin F, Spadoni A. Wave propagation in periodic buckled beams. Part II: Experiments. Wave Motion 2016;66:210-219.

[35] Comité Euro-International du Béton (CEB). Eurocode 8: Design of structures for earthquake resistance - Part 2: Bridges (EN 1998-2). Brussels: CEN; 2005.

[36] Comité Euro-International du Béton (CEB), Fédération Internationale de la Précontrainte (FIP). Model Code 1990. 6th ed. London: Thomas Telford; 1993.

[37] Comité Euro-International du Béton (CEB). Eurocode 2: Design of concrete structures - Part 1-1: General rules and rules for buildings (EN 1992-1-1). Brussels: CEN; 2004.

[38] Vayas I, Iliopoulos A. Design of steel-concrete composite bridges to Eurocode. 1st ed. Boca Raton: CRC Press; 2013.

[39] Brun M, Movchan AB, Slepyan LI. Transition wave in a supported heavy beam. J Mech Phys Solids 2013;61:2067-2085.

[40] Graff KF. Wave motion in elastic solids. 1st ed. New York: Dover Publications, Inc; 1975.

[41] Sonti VR, Narayana TSS. Propagation constants from the response of a finite periodic beam. Noise Control Eng J 2006;54:194-200.

[42] Wen J, Wang G, Yu D, Zhao H, Liu Y. Theoretical and experimental investigation of flexural wave propagation in straight beams with periodic structures: Application to a vibration isolation structure. J Appl Phys 2005;97:114907.